Supplementary Information
Crystal structures and superconductivity of lithium and fluorine implanted gold hydrides under high pressures

Shoutao Zhang*,[a], Qiuping Yang[a], Xiaohua Zhang[a], Kaixuan Zhao[a], Hong Yu[a], Li Zhu*,[d] and Hanyu Liu*,[b,c]

[a]Centre for Advanced Optoelectronic Functional Materials Research and Key Laboratory for UV Light-Emitting Materials and Technology of Ministry of Education, Northeast Normal University, Changchun 130024, China

[b]International Center for Computational Method & Software and State Key Laboratory of Superhard Materials, College of Physics, Jilin University, Changchun 130012, China

[c]Key Laboratory of Physics and Technology for Advanced Batteries (Ministry of Education),College of Physics, Jilin University, Changchun 130012, China

[d]Department of Physics, Rutgers University, Newark, NJ 07102, USA

Corresponding Authors Email: zhangst966@nenu.edu.cn; li.zhu@rutgers.edu; hanyuliu@jlu.edu.cn

Computational Details

Our structural prediction approach is based on a global minimization of free energy surfaces merging *ab initio* total-energy calculations with CALYPSO (Crystal structure AnaLYsis by Particle Swarm Optimization) methodology as implemented in the CALYPSO code.[1,2] The structures of stoichiometry $M_xAu_yH_z$ (M = Li, F; $x = y = 1$, $z = 1 – 6$; $y = z = 1$, $x = 2 – 6$; $y = 1$, $x = z = 2 – 6$; $y = 2$, $x = 1$, $z = 1 – 6$; $y = 2$, $z = 1$, $x = 2 – 6$) were searched with simulation cell sizes up to 4 formula units (f.u.) at 25, 50, and 100 GPa. In the first step, random structures with certain symmetry are constructed in which atomic coordinates are generated by the crystallographic symmetry operations. Local optimizations using the VASP code[3] were done with the conjugate gradients method and stopped when enthalpy changes became smaller than 1×10^{-5} eV per cell. After processing the first generation structures, 60% of them with lower enthalpies are selected to construct the next generation structures by PSO (Particle Swarm Optimization). 40% of the structures in the new generation are randomly generated. A structure fingerprinting technique of bond characterization matrix is applied to the generated structures, so that identical structures are strictly forbidden. These procedures significantly enhance the diversity of the structures, which is crucial for structural global search efficiency. The structural searching simulations for each stoichiometry were stopped after generating 1000 ~ 1200 structures (e.g., about 20 ~ 30 generations).

To further analyze the structures with higher accuracy, we select a number of structures with lower enthalpies and perform structural optimization using density functional theory within the generalized gradient approximation (GGA)[4] as implemented in the VASP code. The cut-off energy for the expansion of wavefunctions into plane waves is set to 800 eV in all calculations, and Monkhorst–Pack k-meshes with appropriate spacing in reciprocal space were adjusted: $2\pi \times 0.025$ Å^{-1} for $Li_xAu_yH_z$ and $2\pi \times 0.03$ Å^{-1} for $F_xAu_yH_z$ structures. This usually gives total energy well converged within ~1 meV/atom. The electron-ion interaction was described by means of projector augmented wave (PAW)[5] pseudopotentials with $5d^{10}6s^1$, $2s^22p^5$, $1s^22s^1$, and $1s^1$ electrons as valence for Au, F, Li, and H atoms, respectively.

The electron-phonon coupling calculations of metallic Li-Au-H compounds are carried out with the density functional perturbation (linear response) theory as implemented in the QUANTUM ESPRESSO package.[6] We employ the ultrasoft pseudopotentials with with $5d^{10}6s^1$, $1s^22s^1$, $1s^1$ as valence electrons of Au, Li, and H atom, respectively. The kinetic energy cutoff for wave-function expansion is chosen as 60 Ry. To reliably calculate electron-phonon coupling (EPC) in metallic systems, we need to sample dense k-meshes for the electronic Brillouin zone integration and

enough q-meshes for evaluating average contributions from the phonon modes. Dependent on specific structures of Li-Au-H compounds, different k-meshes and q-meshes are used: $12 \times 12 \times 9$ k-meshes and $4 \times 4 \times 3$ q-meshes for LiAuH in the $P4/mmm$ structure, $16 \times 16 \times 4$ k-meshes and $8 \times 8 \times 2$ q-meshes for LiAu$_2$H in the $P4/mmm$ structure, $8 \times 8 \times 12$ k-meshes and $4 \times 4 \times 6$ q-meshes for Li$_2$Au$_2$H in the $Cmmm$ structure, $12 \times 8 \times 6$ k-meshes and $6 \times 4 \times 3$ q-meshes for Li$_6$AuH in the $I4/mmm$ structure. We have calculated the superconducting T_c of all the metallic Li-Au-H compounds as estimated from the Allen-Dynes modified McMillan formula[7,8]:

$$T_c = \frac{\omega_{log}}{1.2} exp\left\{ -\frac{1.04(1+\lambda)}{\lambda - \mu^*(1+0.62\lambda)} \right\}, \quad (1)$$

Here, ω_{log} is the logarithmic average phonon frequency, and μ^* is the Coulomb pseudopotential ($\mu^* = 0.1$). The frequency-dependent EPC parameter $\lambda(\omega)$ is calculated by Eliashberg spectral function $\alpha^2 F(\omega)$,

$$\lambda(\omega) = 2\int_0^\infty \frac{\alpha^2 F(\omega)}{\omega} d\omega, \quad (2)$$

with total EPC parameter λ shown in the T_c equation, and

$$\alpha^2 F(\omega) = \frac{1}{2}\sum_j \int_{BZ} \frac{dq}{\Omega_{BZ}} \omega_{qj}\lambda_{qj}\delta(\omega - \omega_{qj})$$

Herein, the integration is over the first Brillouin zone (BZ), with Ω_{BZ} as the volume of the BZ. The $\boldsymbol{q}$ denotes the phonon wave vector. The phonon frequency of mode j at wave vector $\boldsymbol{q}$ is represented by ω_{qj}. The frequency-dependent EPC parameter for mode j at wave vector $\boldsymbol{q}$ is $\lambda_{qj} = \gamma_{qj}/\pi\hbar N_F\omega_{qj}^2$, where the linewidth for mode j at wave vector $\boldsymbol{q}$ is

$$\gamma_{qj} = 2\pi\omega_{qj}\sum_{nm} \int_{BZ} [(dk)/(\Omega_{BZ})]\left|g_{kn,k+qm}^j\right|^2\delta(\varepsilon_{kn} - \varepsilon_F)\delta(\varepsilon_{k+qm} - \varepsilon_F)$$

. N_F is the electronic density of states at the Fermi level. ε_{kn} is the energies of bands with respect to the Fermi level ε_F at $\boldsymbol{k}$. Here, $g_{kn,k+qm}^j$ is the electron-phonon matrix element for the scattering of an electron in band n at wave vector $\boldsymbol{k}$ state to band m at wave vector $\boldsymbol{k}+\boldsymbol{q}$ state via a phonon with wave vector $\boldsymbol{q}$.

Supplementary Figures
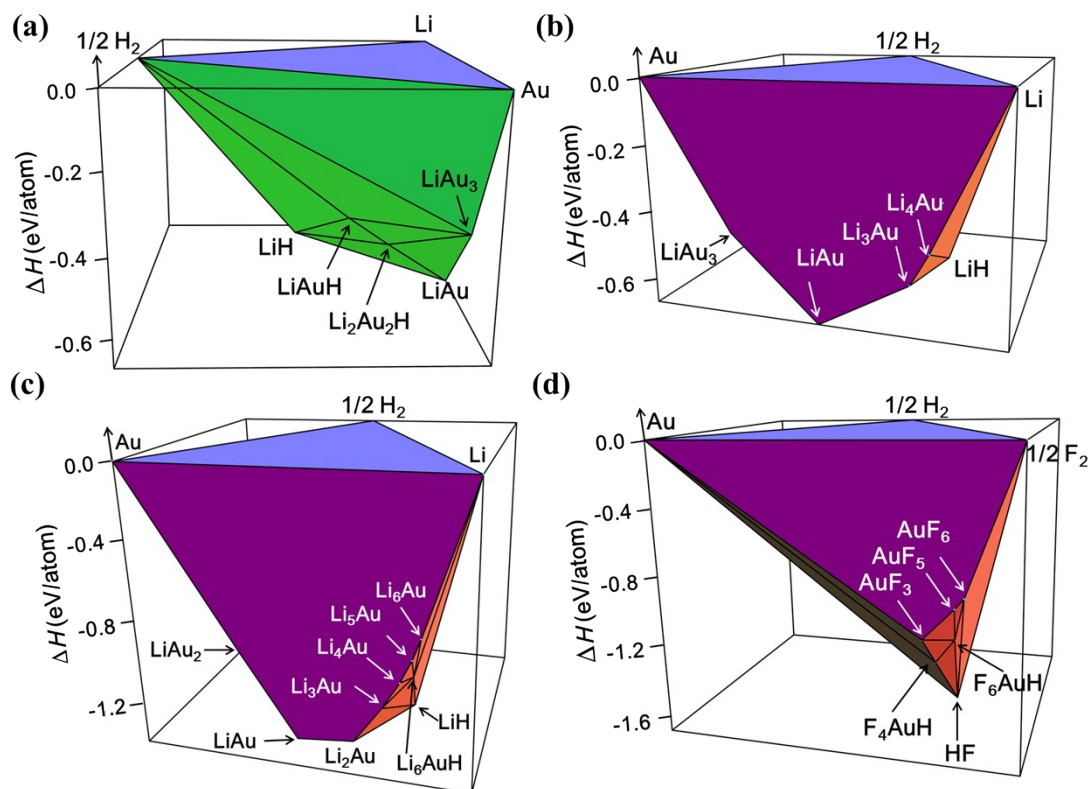
Figure S1. Phase stabilities of (a, b) $Li_xAu_yH_z$ compounds relative to Li, Au, and H_2 at 5 GPa, (c) $Li_xAu_yH_z$ compounds relative to Li, Au, and H_2 at 100 GPa, and (d) ternary $F_xAu_yH_z$ compounds with respect to F_2, Au, and H_2 at 6 GPa.
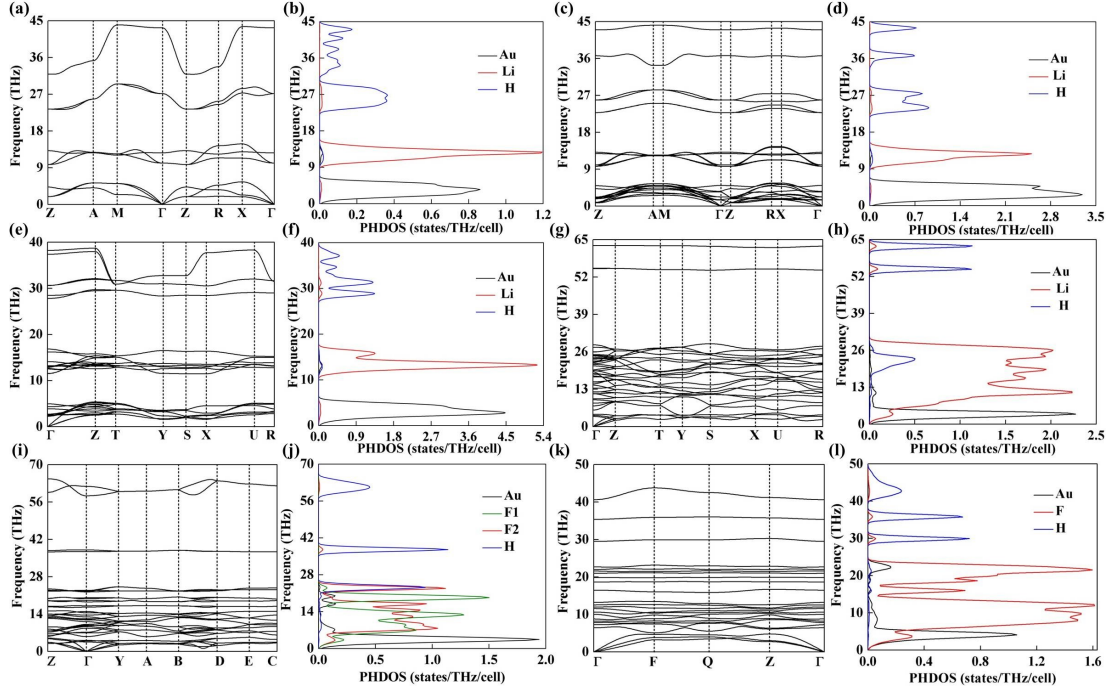
Figure S2. Phonon dispersion curves along the high-symmetry directions in the first Brillouin zone and corresponding projected phonon density of states (PHDOS) of (a, b) $P4/mmm$ LiAuH at 25 GPa, (c, d) $P4/mmm$ LiAu$_2$H at 25 GPa, (e, f) $Cmmm$ Li$_2$Au$_2$H at 25 GPa, and (g, h) $Immm$ Li$_6$AuH at 100 GPa, (i, j) $C2/m$ F$_4$AuH at 50 GPa, (k, l) $P1$ F$_6$AuH at 50 GPa.

(a) *P4/mmm* LiAuH at 25 GPa

(b) *P4/mmma* LiAu₂H at 25 GPa

(c) *Cmmm* Li₂Au₂H at 25 GPa

(d) *Immm* Li₆AuH at 100 GPa

(e) *P*1 F₆AuH at 50 GPa

(f)

Au
Li
F
H
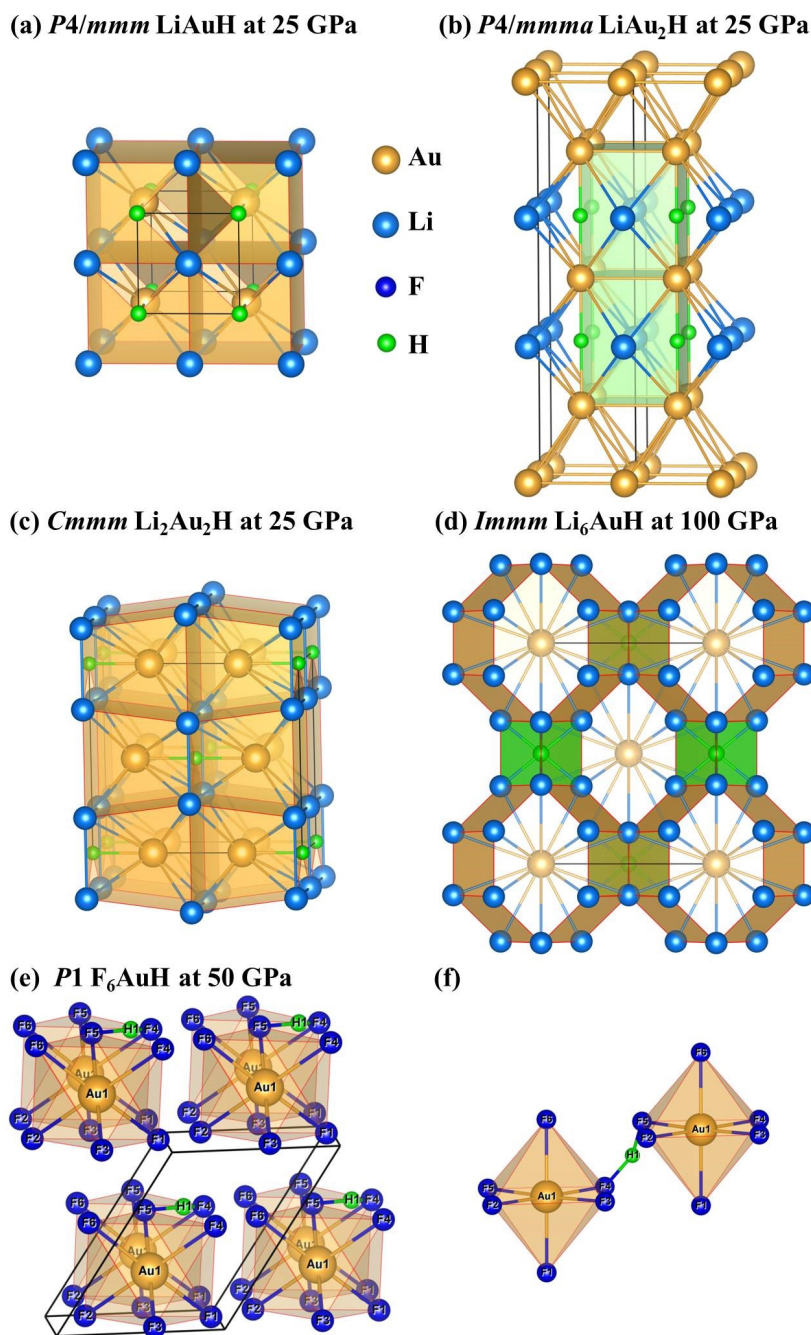
Figure S3. View of polyhedron in (a) *P*4/*mmm* LiAuH, and (b) *P*4/*mmm* LiAu$_2$H, and (c) *Cmmm* Li$_2$Au$_2$H at 25 GPa. (d) View of polyhedron in *Immm* Li$_6$AuH at 100 GPa. View of hydrogen-linked Au-F polyhedrons in (e) *P*1 F$_6$AuH. (f) Local bonding structure in *P*1 F$_6$AuH at 50 GPa. Neighboring interatomic distances: $d_{\text{Au1-F1}}$ = 1.870 XXXÅ, $d_{\text{Au1-F2}}$ = 1.864 Å, $d_{\text{Au1-F3}}$ = 1.861 Å, $d_{\text{Au1-F4}}$ = 1.934 Å, $d_{\text{Au1-F5}}$ = 1.927 Å, $d_{\text{Au1-F6}}$ = 1.891 Å, $d_{\text{F4-H1}}$ = 1.146 Å, and $d_{\text{F5-H1}}$ = 1.143 Å.
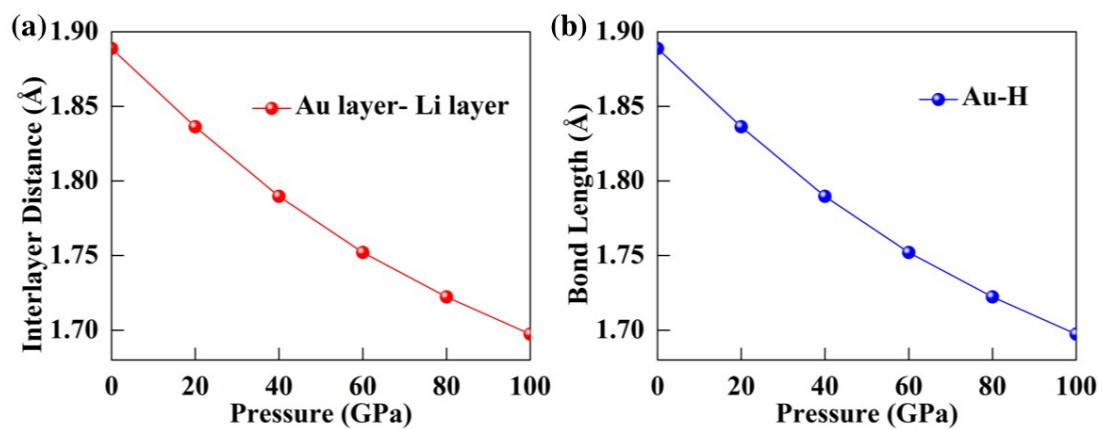
Figure S4. (a) Interlayer distance between Au layer and Li layer in *P*4/*mmm* LiAuH as a function of pressure. (b) Pressure-dependent Au-H bond length in *P*4/*mmm* LiAuH.
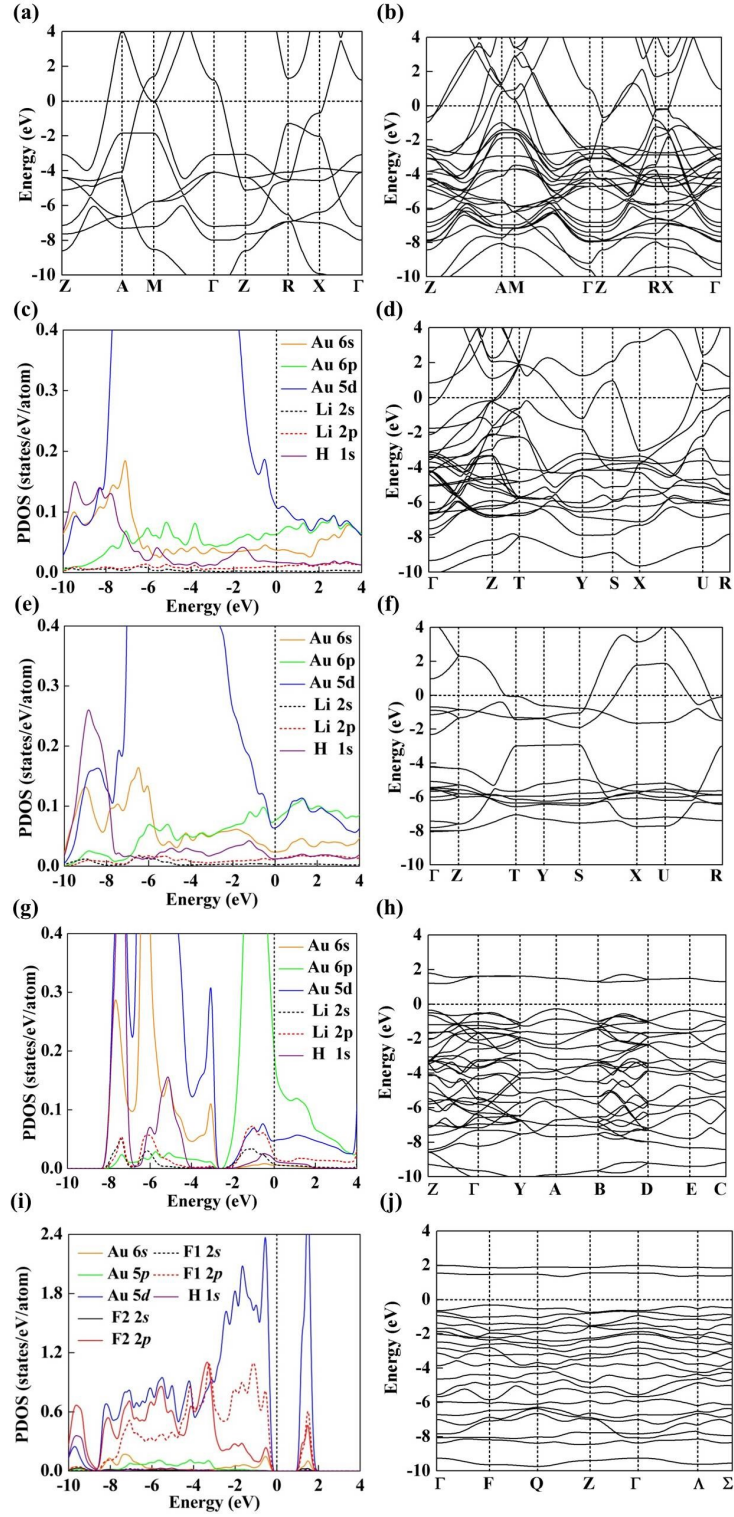
Figure S5. Electronic band structures and corresponding projected density of states (PDOS) of (a) *P4/mmm* LiAuH at 25 GPa, (b, c) *P4/mmm* LiAu$_2$H at 25 GPa, (d, e) *Cmmm* Li$_2$Au$_2$H at 25 GPa, and (f, g) *Immm* Li$_6$AuH at 100 GPa, (h, i) *C2/m* F$_4$AuH at 50 GPa, (j) *P*1 F$_6$AuH at 50 GPa. *P*1 F$_6$AuH has an indirect bandgap of 1.57 eV at 50 GPa.

(a) *P4/mmm* LiAu₂H

(b) *Cmmm* Li₂Au₂H

(c) *P*1 F₆AuH

Au
Li
F
H
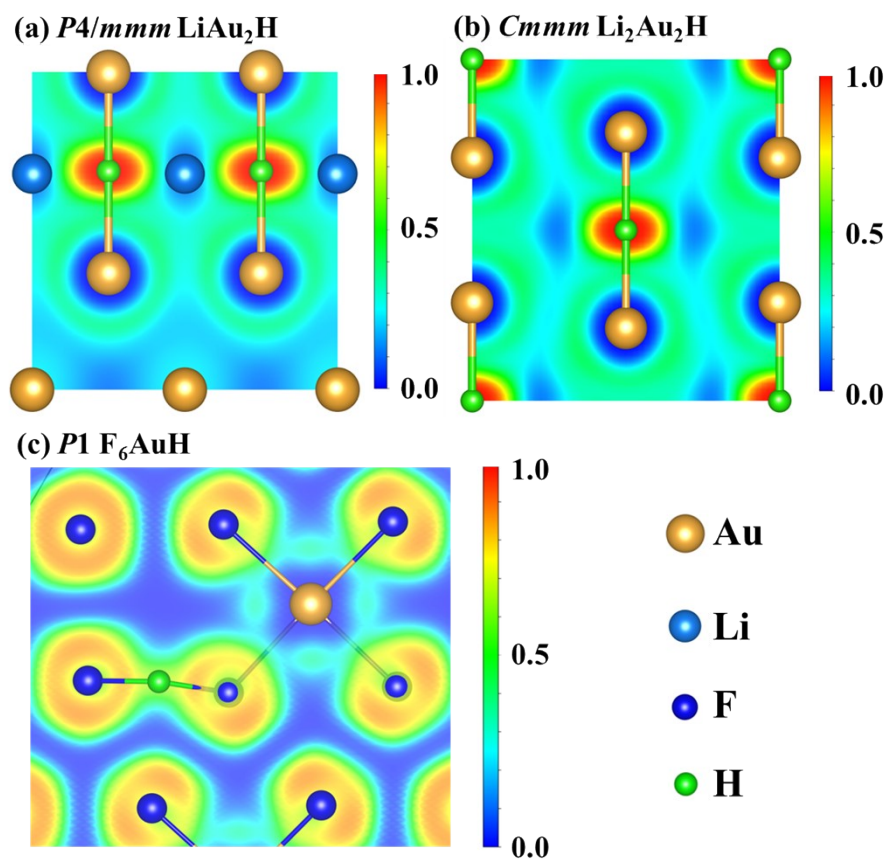
Figure S6. Electron localization function (ELF) of (a) $P4/mmm$ LiAu$_2$H and (b) $Cmmm$ Li$_2$Au$_2$H at 25 GPa. (c) ELF of P1 F$_6$AuH at 50 GPa.
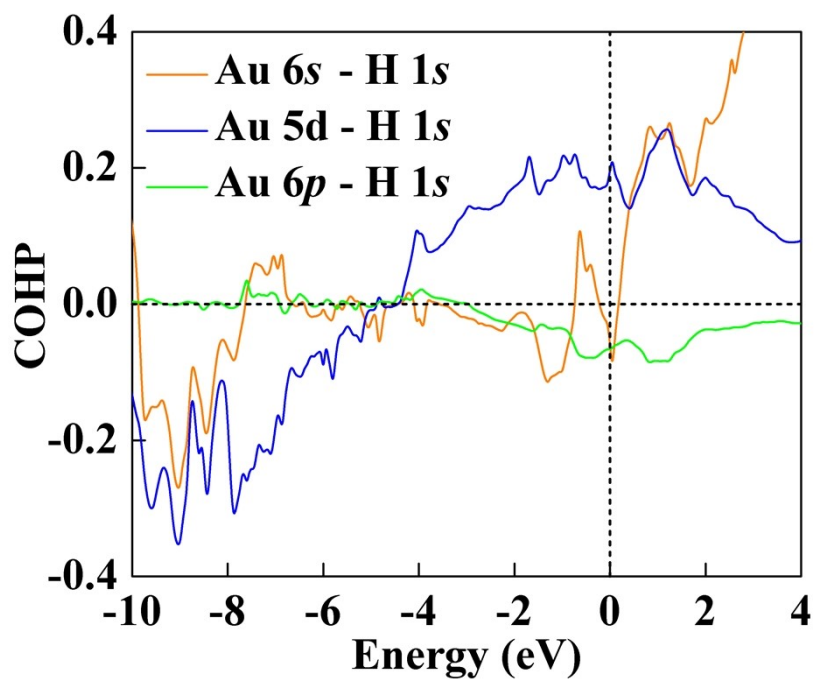
Figure S7. The crystal orbital Hamilton population (COHP) of adjacent Au-H pair in $P4/mmm$ LiAuH at 25 GPa.
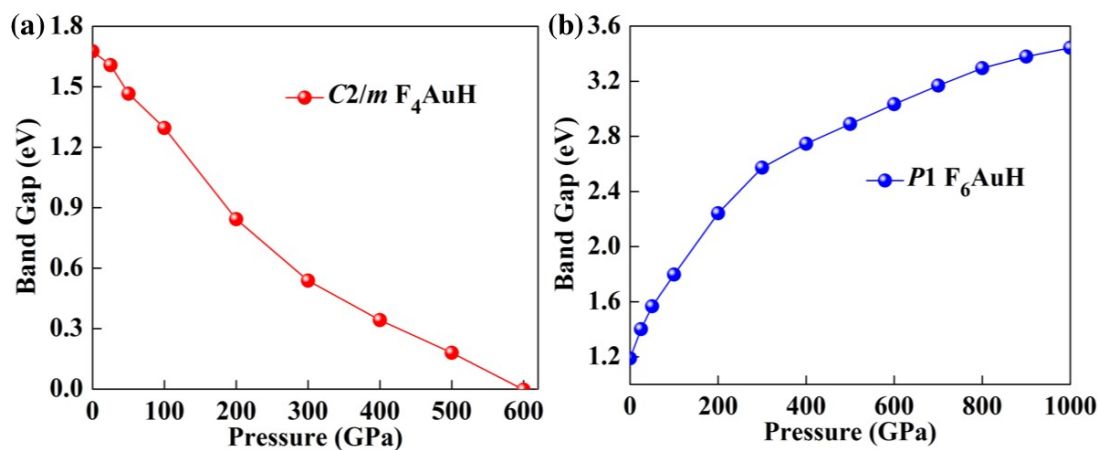
Figure S8. Pressure dependence of band gap for $C2/m$ F_4AuH and $P1$ F_6AuH.
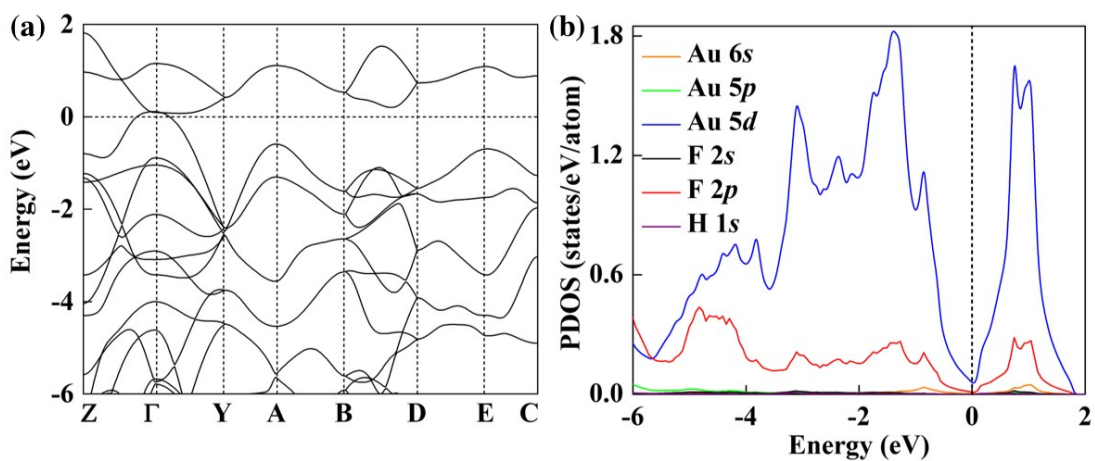
Figure S9. (a) Electronic band structures and (b) corresponding projected density of states (PDOS) of $C2/m$ F_4AuH at 620 GPa.
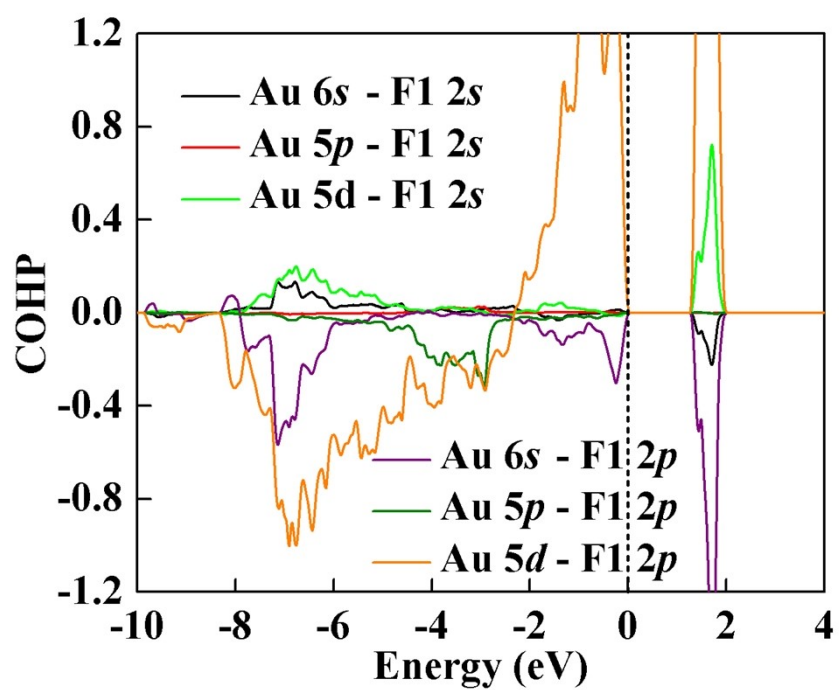
Figure S10. COHP of adjacent Au-F1 and F1-H pairs in *C*2/*m* F$_4$AuH at 50 GPa.

Supplementary Tables

Table S1. Structural parameters of predicted stable Li-Au-H and F-Au-H compounds at selected pressures.

Phases	P (GPa)	Lattice Parameters (Å, °)	Atoms	Wyckoff Positions (fractional) x	y	z
$C2/m$ F$_4$AuH	50	$a = 6.84250$	Au(2a)	0.50000	0.50000	0.00000
		$b = 4.01130$	F(4i)	0.63962	0.00000	0.45036
		$c = 4.96120$	F(4i)	0.18356	0.00000	0.82801
		$\alpha = 90.00000$	H(2c)	0.50000	0.50000	0.50000
		$\beta = 137.23359$				
		$\gamma = 90.00000$				
$P1$ F$_6$AuH	50	$a = 4.30882$	Au(1a)	0.66213	0.86409	0.32596
		$b = 4.28186$	F(1a)	0.12480	0.94078	0.06754
		$c = 4.64145$	F(1a)	0.84543	0.59075	0.06111
		$\alpha = 116.84535$	F(1a)	0.48478	0.32080	0.06424
		$\beta = 118.67422$	F(1a)	0.47682	0.15897	0.59680
		$\gamma = 57.85548$	F(1a)	0.85928	0.39569	0.61487
			F(1a)	0.20609	0.78112	0.60027
			H(1a)	0.62380	0.33138	0.61895
$P4/mmm$ LiAuH	25	$a = 2.73520$	Au(1b)	0.00000	0.00000	0.50000
		$b = 2.73520$	Li(1c)	0.50000	0.50000	0.00000
		$c = 3.64950$	H(1a)	0.00000	0.00000	0.00000
		$\alpha = 90.00000$				
		$\beta = 90.00000$				
		$\gamma = 90.00000$				
$P4/mmm$ LiAu$_2$H	25	$a = 2.75060$	Au(1a)	0.00000	0.00000	0.00000
		$b = 2.75060$	Au(1d)	0.50000	0.50000	0.50000
		$c = 11.43760$	Au(2h)	0.50000	0.50000	0.18321
		$\alpha = 90.00000$	Li(2g)	0.00000	0.00000	0.33976
		$\beta = 90.00000$	H(2h)	0.50000	0.50000	0.34407
		$\gamma = 90.00000$				
$Cmmm$ Li$_2$Au$_2$H	25	$a = 6.41540$	Au(4g)	0.71254	0.00000	0.00000
		$b = 5.77730$	Li(4j)	0.00000	0.21385	0.50000
		$c = 2.74960$	H(2a)	0.00000	0.00000	0.00000
		$\alpha = 90.00000$				

		$\beta = 90.00000$			
		$\gamma = 90.00000$			
Immm Li$_6$AuH	100	$a = 3.09530$	Au(2a)	0.00000	0.00000	0.00000
		$b = 5.00630$	Li(8l)	0.50000	0.73077	0.14867
		$c = 6.30160$	Li(4j)	0.50000	0.00000	0.35834
		$\alpha = 90.00000$	H(2c)	0.00000	0.00000	0.50000
		$\beta = 90.00000$			
		$\gamma = 90.00000$			

Table S2. The integrated crystal orbital Hamilton population (ICOHP) of the neighboring Au-H pair for *P*4/*mmm* LiAuH, *P*4/*mmm* LiAu$_2$H, and *Cmmm* Li$_2$Au$_2$H at 25 GPa.

Phases	Distance (Å)	ICOHP(E_f) (eV/pair)
	Au-H	Au-H
*P*4/*mmm* LiAuH	1.825	-0.300
*P*4/*mmm* LiAu$_2$H	1.783	-0.525
Cmmm Li$_2$Au$_2$H	1.844	-0.220

Table S3. Superconducting properties of ternary Au-Li-H compounds.

Phases	Pressure (GPa)	λ	ω_{log}(K)	$N(E_f)$ (states/Ry)	T_c (K)
*P*4/*mmm* LiAuH	25	□0.36	605.19	2.88	1.30
	50	0.41	496.11	2.87	2.49
	75	0.47	410.35	2.84	3.88
	100	0.51	351.33	2.76	4.69
*P*4/*mmm* LiAu$_2$H	25	□0.27	427.43	9.34	0.06
Cmmm Li$_2$Au$_2$H	25	□0.25	410.00	5.11	0.02
Immm Li$_6$AuH	100	□0.43	451.62	13.57	2.79

Table S4. Calculated Mulliken and Löwdin charge of F, Au, and H in *C*2/*m* F$_4$AuH and *P*-1 F$_6$AuH at 50 GPa.

Phases	Atoms	Mulliken	Löwdin
*C*2/*m* F$_4$AuH	F1	-0.57	-0.53
	F2	-0.50	-0.41
	Au	1.61	1.48
	H	0.52	0.41
*P*1 F$_6$AuH	F1	-0.49	-0.46
	F2	-0.45	-0.41
	F3	-0.45	-0.41
	F4	-0.44	-0.37
	F5	-0.45	-0.37
	F6	-0.51	-0.47
	Au	2.29	2.08
	H	0.50	0.40

Table S5. Calculated Mulliken and Löwdin charge of F and Au in *P*6$_1$22 AuF$_3$ and *Pnma* AuF$_5$ at 1 atm.

Phases	Atoms	Mulliken	Löwdin
*P*6$_1$22 AuF$_3$	Au	1.61	1.49
	F1	-0.54	-0.49
	F2	-0.53	-0.50
Pnma AuF$_5$	Au	2.28	2.10
	F1	-0.50	-0.47
	F2	-0.40	-0.37
	F3	-0.40	-0.37
	F4	-0.50	-0.47
	F5	-0.48	-0.44
	F6	-0.48	-0.44

Table S6. The ICOHP of the neighboring Au-F and F-H pairs for $C2/m$ F_4AuH and $P1$ F_6AuH at 50 GPa.

Phases	Distance (Å)	ICOHP(E_f) (eV/pair)	Distance (Å)	ICOHP(E_f) (eV/pair)	Distance (Å)	ICOHP(E_f) (eV/pair)
	Au-Au	**Au-Au**	**Au-F**	**Au-F**	**F-H**	**F-H**
C2/m **F_4AuH**	Au-Au		Au-F1		F2-H	
	3.927	-0.014	1.909	-2.071	1.107	-3.172
			Au-F2			
			1.970	-1.605		
P1 **F_6AuH**	Au-Au		Au1-F1		F5-H1	
	4.155	-0.019	1.870	-1.832	1.143	-2.878
			Au1-F2		F4-H1	
			1.864	-1.957	1.146	-2.914
			Au1-F3			
			1.861	-1.937		
			Au1-F4			
			1.934	-1.631		
			Au1-F5			
			1.927	-1.519		
			Au1-F6			
			1.891	-1.792		

Table S7. The ICOHP of the neighboring F-H pair for $Cmcm$ HF at 50 GPa.

Phase	Distance (Å)	ICOHP(E_f) (eV/pair)
	F-H	**F-H**
***Cmcm* HF**	1.116	-3.173

References

1   Y. Wang, J. Lv, L. Zhu and Y. Ma, Crystal Structure Prediction via Particle-Swarm Optimization, *Phys. Rev. B Condens. Matter Mater. Phys.*, 2010, **82**, 094116.

2   Y. Wang, J. Lv, L. Zhu and Y. Ma, CALYPSO: A Method for Crystal Structure Prediction, *Comput. Phys. Commun.*, 2012, **183**, 2063–2070.

3   G. Kresse and J. Furthmüller, Efficient Iterative Schemes for Ab Initio Total-Energy Calculations Using A Plane-Wave Basis Set, *Phys. Rev. B Condens. Matter Mater. Phys.*, 1996, **54**, 11169–11186.

4   J. P. Perdew, J. A. Chevary, S. H. Vosko, K. A. Jackson, M. R. Pederson, D. J. Singh and C. Fiolhais, Atoms, molecules, solids, and surfaces: Applications of the generalized gradient approximation for exchange and correlation, *Phys. Rev. B*, 1992, **46**, 6671–6687.

5   P. E. Blöchl, Projector Augmented-Wave Method, *Phys. Rev. B Condens. Matter Mater. Phys.*, 1994, **50**, 17953.

6   P. Giannozzi, S. Baroni, N. Bonini, M. Calandra, R. Car, C. Cavazzoni, D. Ceresoli, G. L. Chiarotti, M. Cococcioni, I. Dabo, A. Dal Corso, S. de Gironcoli, S. Fabris, G. Fratesi, R. Gebauer, U. Gerstmann, C. Gougoussis, A. Kokalj, M. Lazzeri, L. Martin-Samos, N. Marzari, F. Mauri, R. Mazzarello, S. Paolini, A. Pasquarello, L. Paulatto, C. Sbraccia, S. Scandolo, G. Sclauzero, A. P. Seitsonen, A. Smogunov, P. Umari and R. M. Wentzcovitch, QUANTUM ESPRESSO: a modular and open-source software project for quantum simulations of materials, *J. Phys. Condens. Matter*, 2009, **21**, 395502.

7   W. L. McMillan, Transition Temperature of Strong-Coupled Superconductors, *Phys. Rev.*, 1968, **167**, 331–344.

8   P. B. Allen and R. C. Dynes, Transition temperature of strong-coupled superconductors reanalyzed, *Phys. Rev. B*, 1975, **12**, 905–922.